Understanding EUV mask blank surface roughness induced LWR and associated roughness requirement

Pei-yang Yan[1], Guojing Zhang[1], Eric M. Gullikson[2], Kenneth A. Goldberg[2], Markus P. Benk[2]
[1]Intel Corporation, 2200 Mission College Blvd. Santa Clara, CA 95054
[2]Lawrence Berkeley National Lab, 1 Cyclotron Rd., Bldg. 2R0400, Berkeley, CA 94720-8199

ABSTRACT

Extreme ultraviolet lithography (EUVL) mask multi-layer (ML) blank surface roughness specification historically comes from blank defect inspection tool requirement. Later, new concerns on ML surface roughness induced wafer pattern line width roughness (LWR) arise. In this paper, we have studied wafer level pattern LWR as a function of EUVL mask surface roughness via High-NA Actinic Reticle Review Tool. We found that the blank surface roughness induced LWR at current blank roughness level is in the order of 0.5nm 3σ for NA=0.42 at the best focus. At defocus of ±40nm, the corresponding LWR will be 0.2nm higher. Further reducing EUVL mask blank surface roughness will increase the blank cost with limited benefit in improving the pattern LWR, provided that the intrinsic resist LWR is in the order of 1nm and above.

Keywords: Extreme ultraviolet lithography, mask, surface roughness, ML, EUVL, line width roughness, LWR

1. INTRODUCTION

As EUVL application is moving toward 7 nm and beyond technology nodes, many aspects of EUVL mask blank requirements are correspondingly getting tighter. It drives the EUVL cost of ownership higher due to R&D cost and new tool sets requirement to meet new technology specifications. To effectively control the cost of ownership, it is very important to understand and reasonably define all the process error budgets and technology specification requirements. One of the mask blank specifications that we would like to explore for 7 nm and beyond technology node is the EUVL mask ML blank surface roughness. ML blank surface roughness can either be attributed from blank substrate surface roughness or from ML deposition process. The specification for ML surface roughness historically comes from ML blank defect inspection tool requirement. ML surface roughness will cause inspection background noise which reduces the inspection sensitivity. Later, new concerns on ML surface roughness induced wafer pattern line width roughness (LWR) arise.[1-6] Today, the EUVL blank manufactures are able to produce EUVL mask low thermal expansion material (LTEM) substrate with surface roughness in a range of 0.06-0.08nm and ML AFM measured surface roughness in a range of 0.1-0.11nm. The question that we would like to answer in this study is whether further tightening the ML blank surface roughness specification for the purpose of LWR reduction will be beneficial by considering both LWR improvement and cost of ownership of the technology. The surface roughness requirement for the mask inspection purpose will not be addressed in this paper. In this study, we have studied wafer level pattern LWR as a function of EUVL mask surface roughness using the SHARP EUV microscope at Lawrence Berkeley National Lab (LBNL).[7] The pattern LWR is evaluated via actinic aerial images. The advantage of using aerial image evaluation is to separate the ML surface roughness induced LWR from resist intrinsic and process induced LWR which is a dominant source of the total wafer pattern LWR under the current EUV resist process.[8] Our study compares the pattern LWR for different surface roughness conditions at different partial coherence values for NA=0.42. In addition to discussing pattern LWR response to the blank surface roughness under different illumination conditions, we will also present detailed analysis and discussion of pattern LWR response to the mask blank surface roughness at different defocus and different feature sizes. Finally, based on the experimental results, we will discuss the pros and cons of further improving ML surface roughness for future technology nodes.

In section 2, we will discuss EUV ML blank preparation process and present the blank characterization results. In section 3, we will briefly describe the mask design. Section 4 is focused on the experimental results analysis and discussion. The last section is devoted to the conclusions.

Extreme Ultraviolet (EUV) Lithography VI, edited by Obert R. Wood II, Eric M. Panning,
Proc. of SPIE Vol. 9422, 94220J · © 2015 SPIE · CCC code: 0277-786X/15/$18
doi: 10.1117/12.2087041

Downloaded From: http://proceedings.spiedigitallibrary.org/ on 03/23/2015 Terms of Use: http://spiedl.org/terms

2. PROGRAMMED SURFACE ROUGHNESS BLANK PREPARATION

The mask fabrication starts with a blank preparation. A production grade LTEM substrate is first selected. The substrate selected was manufactured by commercial blank vendor in 2010. The substrate AFM measured surface roughness is in the order of ~84pm rms. In order to induce additional surface roughness, we deposited a layer of Cr with gradient thickness along the y-axis on the front side of the LTEM substrate. The film deposition was done at LBNL using magnetron sputtering. The Cr film thickness linearly varies along the Y-axis. The surface roughness of the deposited Cr film linearly varies with the film thickness. The thicker is the film, the rougher is the surface. In order to compare the roughness surface performance with that regular ML blank surface, the Cr deposition area covered only about 2/3 of the mask area along the x-direction as illustrated in Fig. 1. After substrate Cr film deposition, AFM surface roughness measurement along the y-direction at x = -12.5mm in the Cr coated region and at x=37.5mm in the non-coated region are collected. Total of 11 sites with stepping distance of 12mm for both x = -12.5mm and x = 12.5mm positions were measured. The 11 sites along the y-direction are corresponding to the y-locations of each die in the mask pattern design which will be discussed later. The AFM measured Cr surface roughness linear region along the Y-direction ranges from 0.084nm to 1.377nm rms. After Cr film surface roughness AFM characterization, the substrate is then deposited with 40 pairs of Mo/Si ML. The ML deposition was done at SEMATECH, using IBD tool. The ML capping layer is a thin Ru film at thickness ~2.5nm. After ML deposition, the ML surface roughness AFM measurement at the same locations which were collected at the substrate level was performed. In addition, we have also collected EUV reflectivity along the y-direction for both x = -12.5mm and x = 37.5mm, respectively. The EUV reflectivity measurement was done at LBNL.

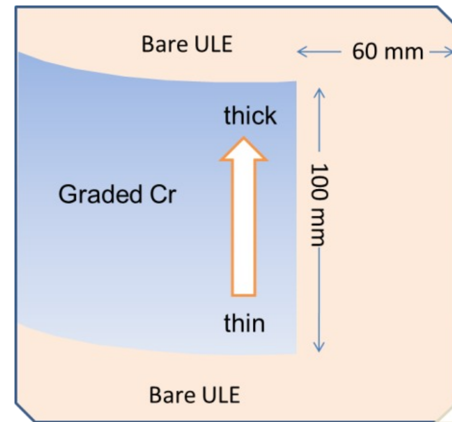

Fig. 1 Schematic plot of gradient Cr deposition scheme (4x mask scale).

In Fig. 2, eight AFM scan images of the LTEM substrate scan in 2umx2um region along the y-direction are given. It can be seen that the Cr surface roughness distribution is rather uniform in the microscopic scale, i.e., no non-uniform singular lager grain size is found.

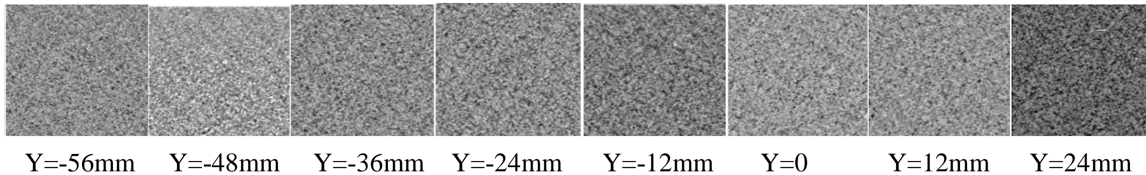

Y=-56mm Y=-48mm Y=-36mm Y=-24mm Y=-12mm Y=0 Y=12mm Y=24mm

Fig. 2 AFM scan images of the LTEM substrate in 2um x 2um region along y-direction.

In Fig. 3a, AFM surface roughness along y-axis in the programmed surface roughness region (x = -12.5mm) for LTEM substrate and ML are given, respectively. In Fig. 3b, the EUV reflectivity measurement along the y-direction for both programmed surface roughness and non-programmed surface region are given, respectively. The AFM surface roughness value in the non-programmed surface roughness region in Fig. 3a showed a similar value as the first roughness value measured in the programmed surface roughness region (y = -60mm). It means there is no Cr film at that location. This can also be seen from Fig. 1 schematic, i.e., no Cr film near the top and bottom of the blank. Based on this result, we will be able to use this location as a plan-of-record (POR) for ML surface roughness reference. In Fig. 3a, it is also shown that ML deposition can effectively smooth out the substrate surface roughness for high substrate surface roughness value. However, such smoothing becomes less effective when the substrate surface roughness value becomes smaller. In fact, at the smallest substrate surface roughness location (AFM roughness value = 0.084nm rms), the ML AFM surface roughness is 0.104nm rms, which is larger than that of LTEM substrate. This phenomenon indicates that ML deposition itself will create its own surface roughness, or intrinsic ML surface roughness which has little to do with the substrate surface roughness. In another word, further ML surface roughness improvement should be focus on ML deposition

Downloaded From: http://proceedings.spiedigitallibrary.org/ on 03/23/2015 Terms of Use: http://spiedl.org/terms

induced surface roughness reduction. Substrate surface roughness reduction will not no longer help to reduce the ML surface roughness.

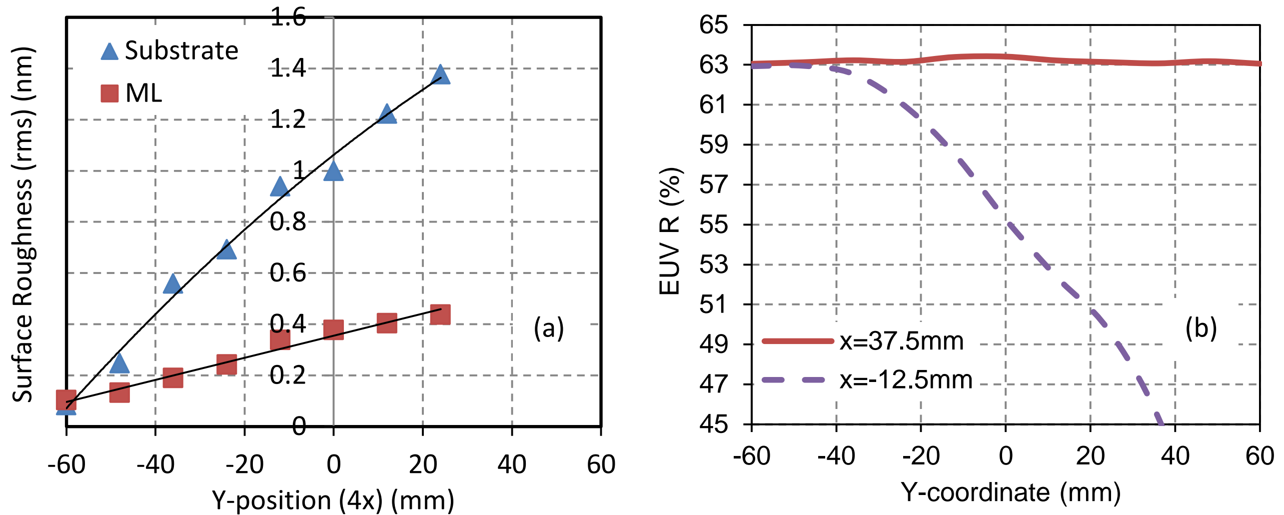

Fig. 3 (a) AFM surface roughness RMS value for LTEM substrate and ML, respectively. (b) EUV reflectometor measurement of ML EUV reflectivity in both programmed and non-programmed surface roughness region, respectively.

It is also shown in Fig. 3b that the ML reflectivity in the programmed surface roughness region decreases as ML surface roughness increases. This is because surface roughness induces EUV light scattering loss. In the region y = -60mm, the reflectivity value is about the same as non-Cr coated region. This is consistent with the AFM result that discussed in the previous paragraph.

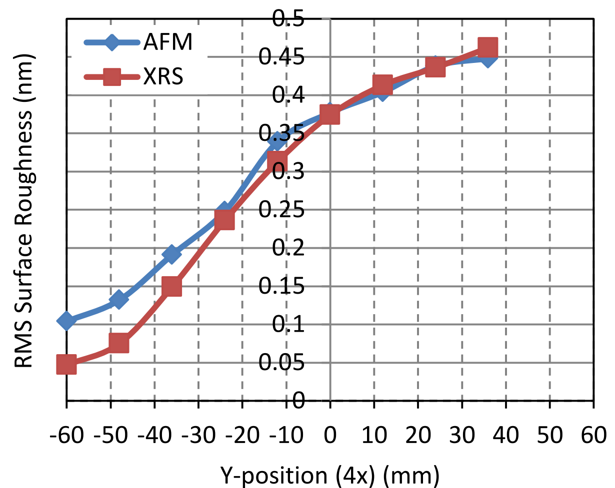

Fig. 4 AFM and EUV scatterometry determined RMS surface roughness as a function of mask y-positions.

Although the LWR is correlated to the AFM measured surface roughness, the ML surface roughness that actually impacts the LWR in EUVL is the so called replicated multilayer surface roughness (RSR). RSR is the roughness which is replicated in at least the top 10 layers of the multilayer stack. The RSR can be determined from EUV scatterometry data, i.e., EUV scattering angular distribution vs. scattering angle. In our experiment, the synchrotron based EUV reflectometer measurement on the blank was performed at LBNL. From the measured scatterometry data, we are able to extrapolate EUV RSR at different Y-locations. In Fig. 4, the plot of ML RMS surface roughness measure by AFM and by EUV scatterometry are given, respectively. It is shown in Fig. 4 that at high roughness region, the AFM measured RMS surface roughness matched well to RSR. In the smoothed region, the RSR is smaller than that of AFM measured RMS surface roughness value. It is worth to point out that this ML blank showed very low RSR surface roughness value of 47pm at the smoothed region (or non-programmed surface roughness region). A constant of 50pm RSR RMS value is specified in the recently updated 2014 ITRS (The International Technology Roadmap for Semiconductors) for future EUV technology nodes.[10]

3. MASK DESIGN AND FABRICATION

The EUV mask absorber used is the combined TaN and TaON anti-reflecting coating at total thickness of 85nm. The film was deposited using in-house sputtering tool. In order to evaluate mask performance at different surface roughness

Downloaded From: http://proceedings.spiedigitallibrary.org/ on 03/23/2015 Terms of Use: http://spiedl.org/terms

values, we design the mask pattern layout as 5x11(col x row) identical fields (i.e., 5 fields along the x-direction and 11 fields along the y-direction) as shown in Fig. 5. Each region has the identical pattern design. The y-stepping distance between the adjacent fields is 12mm on the mask. Three left columns fall into the programed roughness region and two right columns are in the non-programmed surface roughness region. Although we have designed redundant columns for both programmed and non-programmed surface roughness regions, in this study, we only focused on column number 3 for the programmed region. As indicted in Fig. 1, the upper part of the mask has thicker film, therefore, rougher than that of the lower part of the mask. The 11 sites from top to bottom are labeled as site 1 to 11 as indicated in Fig. 5. Site 11 falls into the non-Cr coated region.

The mask pattern design consists of series of lines spaces, and contacts at different sizes. In the study, we focus on dense line LWR response to the different region of ML which corresponds to different surface roughness.

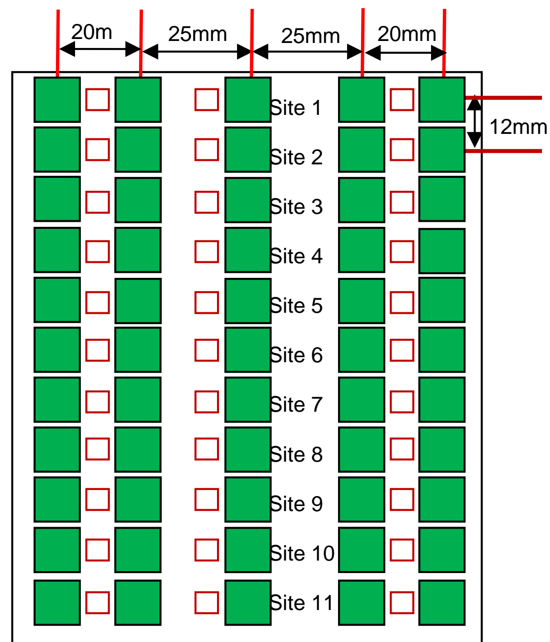

Fig. 5 Schematics of mask pattern layout.

4. EXPERIMENTAL RESULTS AND DISCUSSIONS

As we have discussed earlier, the main purpose of this study is to understand the impact of the current ML quality blank surface roughness to pattern LWR and to assess the need for further surface roughness improvement when necessary. However, since the current high quality ML blank typically has AFM surface roughness in the order to 0.1nm, we will not be able to directly obtain the ML surface roughness impact to wafer LWR for ML surface roughness below 0.1nm. With the program surface roughness design which provides a series surface roughness values, we hope that we can obtain a trend as how LWR response to the surface roughness so that we can understand ML surface roughness effect at even smaller surface roughness value. Previously, experimental study of ML surface roughness to wafer level LWR via wafer printing has been performed by Vaglio Pret et al.[8] Unfortunately, the effect of surface roughness induced LWR can only be seen in the experiment at larger surface roughness values. This is because that in such experiment, the resist LWR is dominating the total LWR. As the total observed LWR is the quadrature sum of all the contributors, e.g., mask LWR, surface roughness induce LWR, resist LWR, etc. when one of the contributors induced LWR is much larger than that of others, the small contributor's contribution will not be able to observed readily. Bhattarai et al has performed a simulation study and conclude that the surface roughness induced LWR is only 1.3% of the total LWR in wafer printing with current chemical amplified resist.[9] In our experiment, we used actinic aerial image to evaluate LWR, there will be no resist LWR impact. In fact, in the experiment, we are able to observed LWR response to the surface roughness down to the minimum surface roughness value available. However, we have encountered similar dilemma at lower surface roughness region, i.e., at low surface roughness, the shot noise induced LWR become quite noticeable. This effect has been studied previously for actinic imaging.[11] We have initially under estimated the effect of shot noise contribution to the experiment and used standard exposure time of 5 seconds for the throughput consideration. With 5 seconds exposure time, we have observed quite large LWR contribution at all level of surface roughness values. Later, we increased the exposure time to 20 and 30 seconds to minimize the shot noise effect. Due to limited tool time available for this experiment, we were not able to repeat the imaging with even longer exposure time. More discussion on the shot noise impact to the experiment result will be discussed in the later sections.

4.1. Data collection and analysis method

In the experiment, we have focused on imaging both 26nm L/S and 20nm L/S (1x) at NA=0.42 with two partial coherence values of 0.3 and 0.7, respectively. At each die (or site), a series of actinic images of the same features design are collected at illumination wavelength of 13.5nm with different focus. The image analysis is confined in an area of 3µm x 3µm (4x) field-of-view, centered at optics "sweet spot" which provides the best alignment and minimum lens aberration. For 26nm L/S pattern within 3µm (4x) square field-of-view, we are able to capture 14 lines. For each line,

Downloaded From: http://proceedings.spiedigitallibrary.org/ on 03/23/2015 Terms of Use: http://spiedl.org/terms

we collect LWR information along the full 3μm length. By examining LWR values for each line within the field-of-view, we have noticed somewhat large LWR variation. In order to get more consistent LWR value, for all the LWR analysis, we dropped 3 smallest and 3 largest LWR values among all measured lines. The final LWR value is the average LWR measured from the remaining lines.

4.2 Analysis of surface roughness induced LWR at the best focus

In Fig. 6, aerial images of 26nm L/S under EUV actinic illumination at different sites which corresponds to different surface roughness values are given. It is clearly shown the surface roughness impact in EUVL to wafer lever pattern LWR. The good news is that at the current POR ML surface roughness site #11, lines appeared to be very smooth. In

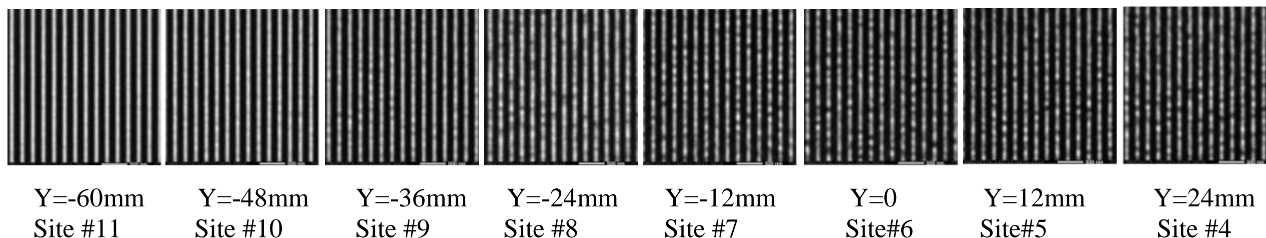

Fig. 6 Actinic images of 26nm L/S at different surface roughness regions for NA=0.42, σ =0.3 and exposure time=5 seconds.

Fig. 7a, the quantitatively measured 26nm dense line LWR from actinic aerial images as a function of ML RSR RMS surface roughness for NA=0.42, partial coherence σ=0.3 and σ=0.7 are given, respectively. The actinic images were collected with 5 seconds exposure time. In Fig. 7b, similar plots are given for the same NA and partial coherence

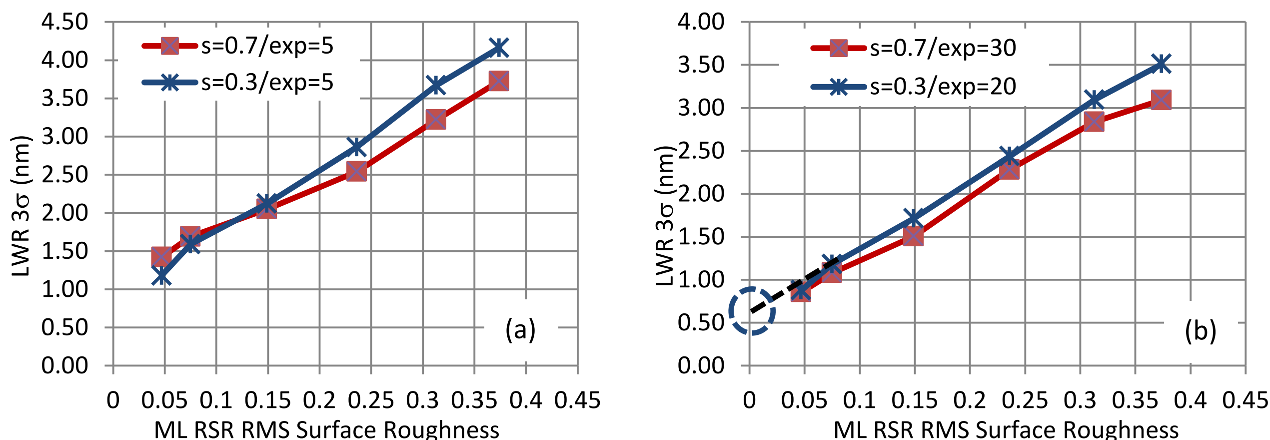

Fig. 7 Plot of total measured LWR for 26nm L/S as a function of ML RSR RMS surface roughness at zero defocus, (a) at exposure time of 5 seconds, (b) at exposure time of 20 seconds for σ=0.7 and 30 seconds for σ=0.3.The dotted line is the trend line for σ=0.3 to reach to zero RMS value. The dotted circle highlights the LWR value at zero RSR. It indicated that even at longer exposure time, The LWR does not trend to zero at zero RSR.

conditions, except the exposure time is 20 seconds for σ=0.3 and 30 seconds for σ=0.7. The aerial image data used in Fig. 7a was collected in the same day and the data used in Fig. 7b also collected in the same day. The data in Fig. 7a and Fig. 7b are collected in the two different days. The actinic imaging tool is not a production tool, it has day-to-day performance variations. In Figs. 7a and 7b, each corresponding data point was collected at the same mask location, i.e., the same mask surface roughness value. The difference seen between Fig. 7a and 7b can attribute to the follow two factors: 1) exposure time difference, 2) day-to-day EUV beamline intensity variation and scan uniformity variation. The exposure time difference translates to photon intensity difference in the exposed mask region. In the case of longer exposure time, the shot noise will be smaller than that of shorter exposure time, or the signal-to-noise will be higher for longer exposure time. The LWR different seen between Fig. 7a and 7b for both high surface roughness and low surface

Downloaded From: http://proceedings.spiedigitallibrary.org/ on 03/23/2015 Terms of Use: http://spiedl.org/terms

roughness regions indicates that the shot noise induced LWR is not independent, but coupled with surface roughness induced LWR. This is understandable since the shot noise will degrade the aerial image quality, and the surface roughness induced LWR is correlated to the aerial image quality. The poorer is the aerial image quality, the lager is the LWR for a given surface roughness value. To further illustrate this point, we extrapolated the aerial image contrast in each case. In Fig. 8a, a comparison plot of aerial image contrast as a function of ML RSR surface roughness at σ=0.3 and exposure time of 5 seconds and 30 seconds is given. In Fig. 8b, a similar comparison plot for σ=0.7 is given. It is shown in both graphs that shot noise reduces aerial image contrast, or quality. As a result, in additional to shot noise

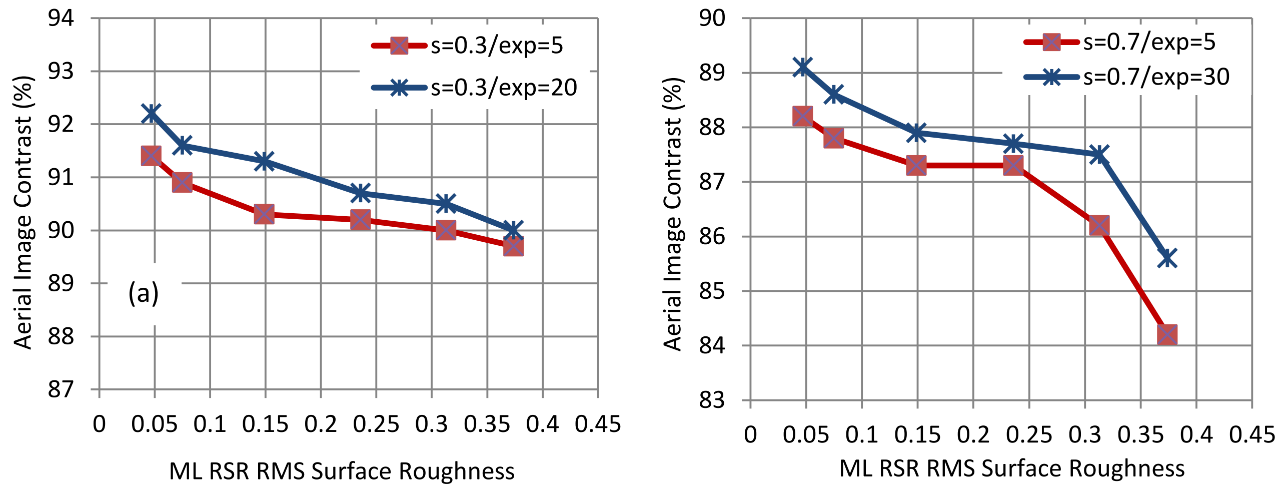

Fig. 8 Plot of contrast as a function of ML RSR surface roughness at different exposures at zero defocus, (a) σ =0.3, and (b) σ =0.7.

contribution to the LWR (e.g., assume a perfect mask with no surface roughness), the surface roughness induce LWR will also increase at larger shot noise value as a result of aerial image degradation. It is worth to point out that when we trend the LWR response to the surface roughness down to zero RSR value, the corresponding LWR value in both Figs. 7a and 7b do not trend to zero, indicting the existence of other LWR contributors in the experiment. More discussion on other LWR contributors in the experiment will be discussed in later sections.

From Figs, 8a and 8b, it is also shown that the aerial image contrast is consistently higher for σ=0.3 than that of σ=0.7. Since high coherence illumination will enhance speckle effect from the surface roughness, we would expect that the total LWR is higher for σ=0.3 case. This is consistent with the results seen in Figs. 7a and 7b at high surface roughness value. At low surface roughness value, we observed that LWR is actually smaller for σ=0.3 than that of σ=0.7 for exposure of 5 seconds case. Although the LWR value is similar at low surface roughness region for both σ=0.3 and σ=0.7 in Fig. 7b, we believe that σ=0.3 case should be slightly better (i.e., similar to that of 5 seconds exposure case in Fig. 7a) if the exposure time for σ=0.3 is also 30 seconds, instead of 20 seconds. The result that σ=0.3 is slightly better at low surface roughness region indicated that when the surface roughness value is low enough, the benefit of mask imaging LWR improvement from aerial image quality improvement overwrites the enhanced speckle effect due to high partial coherence illumination.

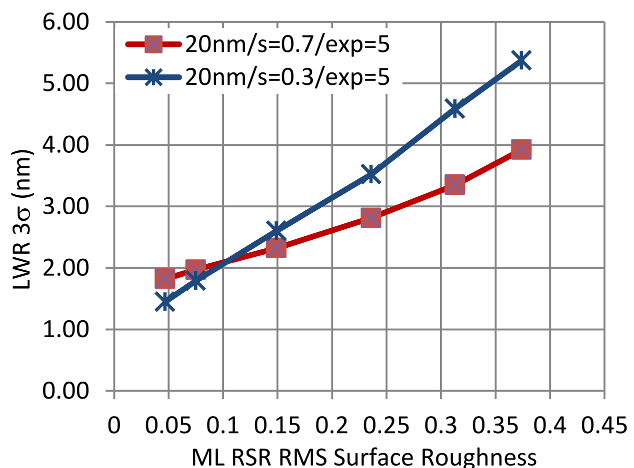

Fig. 9 Plot of 20nm L/S LWR as function of ML RSR surface roughness at zero defocus for σ=0.3 and σ =0.7,

Next, we studied the LWR response to the surface roughness for a smaller feature size of 20nm dense lines.

Downloaded From: http://proceedings.spiedigitallibrary.org/ on 03/23/2015 Terms of Use: http://spiedl.org/terms

The LWR versus ML surface roughness plot is given in Fig. 9. The aerial images were collected at NA=0.42, exposure time of 5 seconds, σ=0.3 and σ=0.7, respectively. The LWR response to the surface roughness trend in the two curves in Fig. 8 is similar to that obtained in Fig. 7. It also showed that higher LWR at higher surface roughness region and lower LWR at low surface roughness region for σ=0.3 when compared to that of σ=0.7 case, i.e., when surface roughness is low, the advantage of aerial image quality enhancement overwrites the effect of speckle enhancement due to high partial coherence. By comparing the LWR value in Fig. 9 with that in Fig. 7a, we found that the LWR value at smoothed region is slightly higher for 20nm than that for 26nm. This is due to the aerial image contrast, which will impact both the surface roughness and shot noise induced LWR, is lower for 20nm that that of 26nm.

4.3 Analysis of Surface roughness induced LWR at defocus condition

In lithography system, when the aerial image is out of focus, its quality degrades and limits the CD process window or depth of focus (DOF). The LWR, regardless of its origin, will also be getting worse. In our experiment, we expect that the observed LWR increase also comes from previously mention three sources, i.e., surface roughness, shot noise, and mask LWR. In Fig. 10a, we plot 20nm L/S LWR at site 11, site 9, and site 7 as a function of defocus for NA=0.42, σ=0.3. In Fig. 10b, the similar plot for σ=0.7 is given. The exposure time for these set of data was 5 seconds. In both

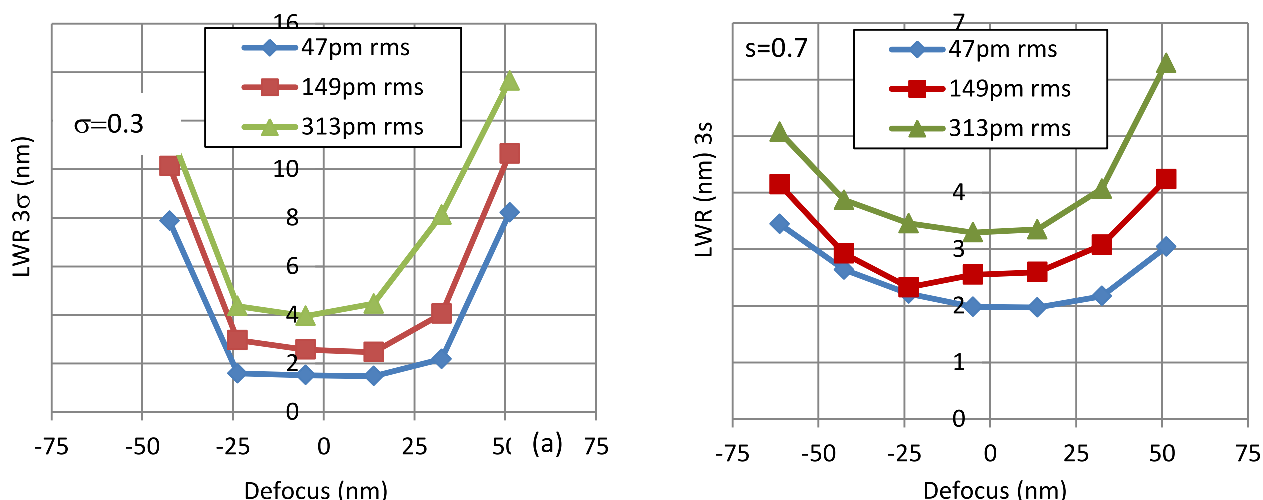

Fig. 10 Plot of LWR as function of defocus for three different ML RSR surface roughness values, (a) for σ=0.3 and (b) σ=0.7. The feature size is 20nm and NA used is 0.42. The data collection exposure time is 5 seconds.

partial coherence cases, the LWR increases with defocus. To further understand the meaningful defocus range, we need to know the CD process window. In Fig. 11, we plot the 20nm L/S CD percentage exposure latitude as a function of DOF at site 11for NA=0.42, σ=0.3 and 0.7, respectively. According to Fig. 11, for 10% exposure latitude, we obtained DOF of 65nm and 87nm, for σ=0.3 and σ=0.7, respectively. Within these DOF ranges, the LWR increased about 1nm for σ=0.3 case and 0.6nm for σ=0.7 case at site 11 (the best surface roughness region). As mentioned earlier, the amount of LWR increase shown in each site is not solely the result of surface roughness. It is the combined effect of surface roughness, shot noise, and mask LWR. Although it is difficult to completely separate these effects, we can further obtain additional information regarding other LWR contribution by looking at LWR as a function of surface roughness trend lines, similar to Fig. 7b for different focus values. In Figs 12a and 12b, such plot for σ=0.3 and

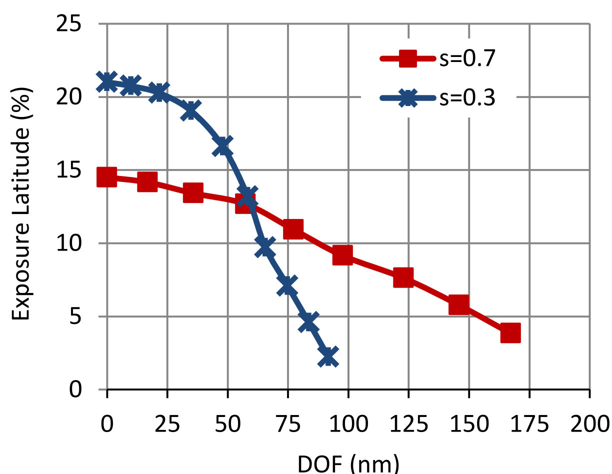

Fig. 11 Plot of 20nm line CD percentage exposure latitude as a function of DOF for σ=0.3 and σ=0.7, respectively.

Downloaded From: http://proceedings.spiedigitallibrary.org/ on 03/23/2015 Terms of Use: http://spiedl.org/terms

σ=0.7 are given, respectively. From these plots, if we draw a trend line to zero surface roughness value from +/-40nm defocus curves, we will not reach zero LWR at zero surface roughness value. This means that the large LWR contribution at defocus seen in the experiment is not coming from mask surface roughness, but other sources, most likely from the shot noise. One of the important outcomes from these two graphs is that the slope of each line at different defocus is similar, indicating amount of LWR improvement by improving surface roughness will be similar at different defocus.

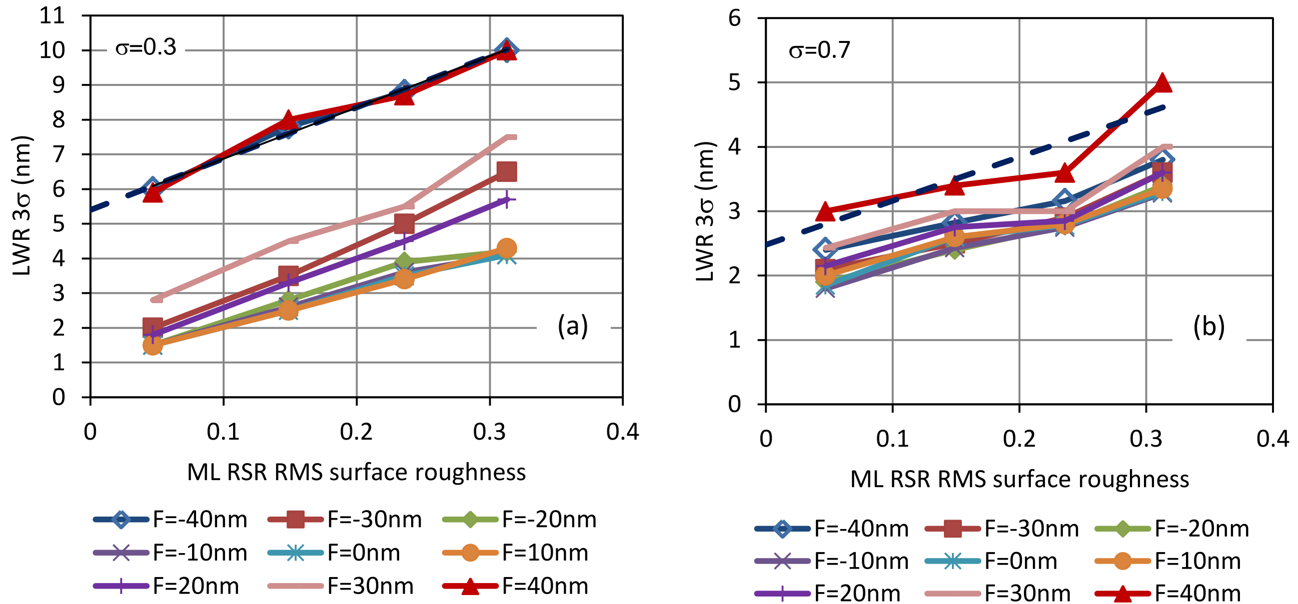

Fig. 12 Plot of LWR as function of ML RSR RMSsurface roughness for different defocus (a) for σ=0.3 and (b) σ=0.7. The feature size is 20nm and the NA used is 0.42. The data collection exposure time is 5 seconds.

4.4 Analysis of Surface roughness induced LWR the best surface roughness location

One of the important outcomes from this study is to understand the impact of the surface roughness induces LWR at the current blank quality. In this experiment, such quality surface roughness region lies in site #11, or approximately y=-60nm. Although we have experimentally obtained LWR values for different illumination conditions at site # 11, we cannot conclude that such LWR values are just induced by ML surface roughness. We have learned during the experiment that when exposure time is short, e.g., 5 seconds, the shot noise contribution to LWR at site #11 can be comparable to that of induced by surface roughness. To further understand the LWR contribution from surface roughness, we need to first understand the shot noise impact. We conducted a series aerial image collection for 26nm L/S at non-programmed surface roughness region for NA=0.42 and σ=0.3 and 0.7 at exposure time of 5, 10, 20, and 30 seconds, respectively in the same day. In Fig. 13, the actinic aerial images of 26nm L/S captured with 5 seconds and 30 seconds exposure time are given, respectively. It can be seen from the pictures that 5 seconds exposed image lines are rougher than that of 30 seconds captured. By further analyzing LWR of the aerial images obtained

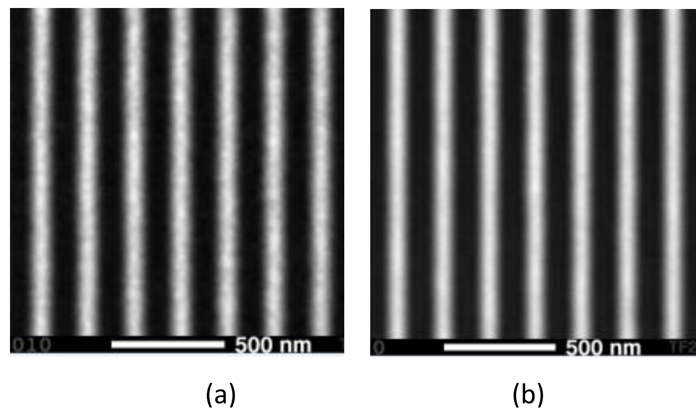

Fig. 13 Actinic images of 26nm L/S. NA=0.42, σ=0.3, (a) exposure time = 5 seconds; (b) exposure time = 30 seconds.

Downloaded From: http://proceedings.spiedigitallibrary.org/ on 03/23/2015 Terms of Use: http://spiedl.org/terms

at different exposure times, we are able to obtain LWR as a function of exposure time. In Fig. 14, such plot is given. It is clearly shown the impact of the shot noise to the LWR. We have noticed that the LWR values at exposure time of 5 seconds, 20 seconds, and 30 seconds not exactly matched to that obtained in Figs. 7a and 7b. The different can be attributable to experimental variations, including day-to-day tool performance variation. As a result, we will be focusing on the relative comparison for the aerial images at different illumination condition obtained in the same day to minimize day-to-day experimental variations. For example, the data in each single graph (e.g., Figs. 7a, 7b, and 9) are collected in the same day. The data in different graphs are collected at different days. From Fig.14, although the LWR drastically trends down when the exposure time increases, it did not reach plateau even at exposure time of 30 second. This means that the LWR values which is about 0.9nm 3σ for 20 seconds or 30 seconds exposure time shown in Fig. 7b is not necessarily the surface roughness contribution alone, but also the shot noise contribution.

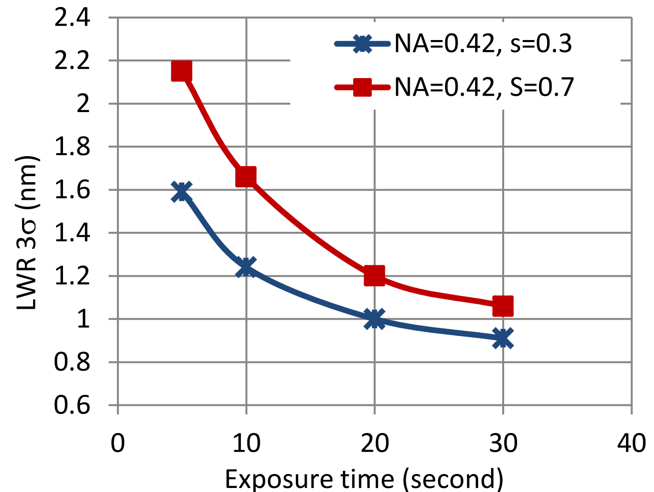

Fig. 14 Plot of 26nm L/S LWR as function exposure time for NA= 0.42, σ=0.3 and 0.7, respectively.

As we have mentioned in the previous section, we cannot cleanly separate the shot noise induced LWR and surface roughness induced LWR as they are coupled together. Even with a perfect mask, the shot noise causes an additional fluctuation to the exposure distribution which is stochastic due to random scattering of the photons. In addition, the shot noise can degrade aerial image quality. This effect can be seen in Fig. 15, where the aerial image contrast as function of exposure time is given. In Fig. 15, we observed that the aerial image contrast decreases as the shot noise increase (shorter exposure time). In the existence of surface roughness, a poor aerial image quality will induce more LWR for a given surface roughness value. Therefore, the surface roughness contribution to LWR is also depending upon shot noise.

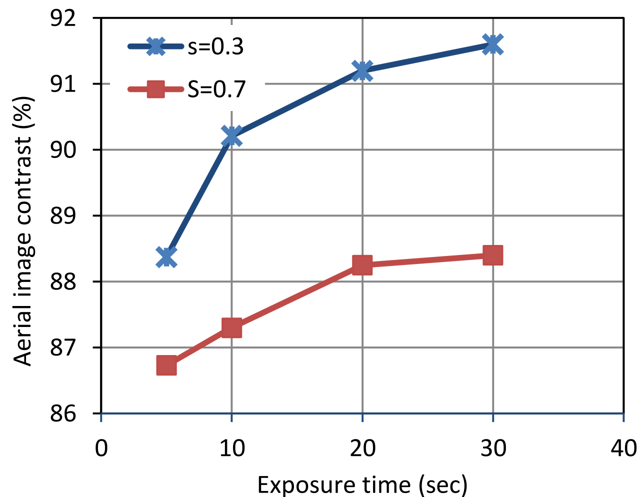

Fig. 15 Plot of 26nm aerial image contrast as a function of exposure time for NA=0.42, σ=0.3 and 0.7, respectively.

In an effort to separate the surface roughness induced LWR from that other contributors, we resort to the plots in Figs 7, 8, and 12. In these graphs, we observed a good linear response of the LWR to the ML surface RSR all the way to the best surface roughness site. By drawing a linear trend lines for these curves down to the zero RSR value, we obtain a LWR value which is independent of ML RSR for each curve. This LWR value is resulted from other sources which we have mentioned a few in the paper. In fact, the exactly partition of LWR contributors is not important. From each linear trend line, we will be able to obtain a corresponding slope, which will tell us how LWR responses to the pure ML RSR by setting zero LWR at zero ML RSR. In Table 1, trend line slopes obtained from Figs. 7, 8, and 12 are given. From these slope values, we can further calculate the pure ML RSR induce LWR at a given ML RSR value. This result is given in Table 2. In the experiment, out ML RSR RMS value of the non-Cr coated region is about 0.047nm (the highlighted row). According to the Table 2, the ML RSR induced the LWR will be in the order of 0.35-0.45nm at the best focus and 0.6nm at 40nm defocus.

Downloaded From: http://proceedings.spiedigitallibrary.org/ on 03/23/2015 Terms of Use: http://spiedl.org/terms

Table 1. Trend line slope of LWR vs. ML RSR for different exposure conditions and feature sizes obtained from Figs. 7, 9, and 12.

Slope of LWR vs ML RSR [(LWR(nm)/RSR rms)]			
		F=0	F=40nm
26nm L/S	σ=0.3/5sec	8.95	14.77
	σ=0.7/5sec	6.8	6.83
	σ=0.3/20sec	8.05	
	σ=0.7/30sec	7.09	
20nm L/S	σ=0.3/5sec	11.88	
	σ=0.7/5sec	6.22	

Table 2 Extrapolated ML RSR induced LWR for 20nm and 26nm L/S at different partial coherence σ and focus values based on Figs. 7, 9, and 12. The slope values used in the calculation are from Table 1.

	slope=8.95	slope=6.8	Slope=8.05	Slope=7.09	Slope=11.88	Slope=6.22	Slope =14.77
RSR (nm)	LWR 3σ (nm)						
0.000	0.00	0.00	0.00	0.00	0.00	0.00	0.00
0.010	0.09	0.07	0.08	0.07	0.12	0.06	0.15
0.020	0.18	0.14	0.16	0.14	0.24	0.12	0.30
0.030	0.27	0.20	0.24	0.21	0.36	0.19	0.44
0.040	0.36	0.27	0.32	0.28	0.48	0.25	0.59
0.050	0.45	0.34	0.40	0.35	0.59	0.31	0.74
0.060	0.54	0.41	0.48	0.43	0.71	0.37	0.89
0.065	0.58	0.44	0.52	0.46	0.77	0.40	0.96
0.070	0.63	0.48	0.56	0.50	0.83	0.44	1.03
0.080	0.72	0.54	0.64	0.57	0.95	0.50	1.18

The ML blank we used in the experiment has a very smooth surface. The current ML blank AFM surface roughness ranges from 0.10-0.12nm rms. According to Fig. 4, this AFM roughness range translates to 0.05-0.07nm RSR RMS values. In Table 2, for the worst case of 0.07nm RSR, the corresponding LWR will be 0.83nm and 1.03nm at the best and at 40nm defocus, respectively.

In today's EUVL, it is well known that the resist intrinsic LWR (i.e., assuming a perfect mask) is a major LWR contributor. In future, resist LWR is expected to be reduced further. However, LWR reduction prefers lower sensitivity resist to reduce the shot noise effect. While EUV tool needs high photon sensitive resist fulfilling the throughput requirement. Therefore, it is very challenging to meet resist photo sensitivity and LWR simultaneously, as many of the traditional methods for increasing sensitivity have been shown to have a negative impact on LWR. Although we can specify resist LWR requirement for each generation of lithography technology, we do not know the ultimate resist LWR that can be achieved in future. It is possible to reduce the pattern LWR via post resist patterning process, including resist post exposure treatment, etch, etc. These post resist pattern method typically can help overall resist LWR, i.e., not only the intrinsic resist LW, but LWR resulted from all sources.

In Table 3, we have estimated total LWR improvement by improving ML surface roughness at the existence of resist induced LWR. In the calculation, the LWR contribution from mask LWR is assumed to be a constant value of 0.2nm. The total LWR is a quadrature sum of the three contributors: resist, mask LWR, and mask surface roughness. The last column in Table 3 shows the total LWR improvement by improving ML RSR surface roughness from 0.07nm to

Downloaded From: http://proceedings.spiedigitallibrary.org/ on 03/23/2015 Terms of Use: http://spiedl.org/terms

0.05nm. This calculation is clearly shown that the amount of improvement by reducing surface roughness depends on the resist LWR contribution, especially when resist LWR is larger than that of from surface roughness. In this case, the total LWR improvement is limited by surface roughness improvement. For example, for resist LWR of 1.5nm, the LWR improvement obtained by further reducing surface roughness from 0.07nm to 0.05nm is only ~0.1nm 3σ. Although in any cases, the lower is the surface roughness the better is the total LWR, we will also need to consider the tradeoffs between the improvement cost, which will translate to the blank cost, and the benefit obtained.

Table 3. Estimated LWR improvement by improving ML RSR surface roughness from 0.07nm to 0.05nm.

Total LWR 3σ (nm)						
From mask LWR	From resist	From surface roughness		Total (quadrature sum)		Improvement
		RSR=0.05nm	RSR=0.07nm	RSR=0.05nm	RSR=0.07nm	RSR (0.07)-RSR (0.05)
0.2	2	0.59	0.83	2.09	2.17	0.08
0.2	1.75	0.59	0.83	1.86	1.95	0.09
0.2	1.5	0.59	0.83	1.62	1.73	0.10
0.2	1.25	0.59	0.83	1.4	1.51	0.12
0.2	1	0.59	0.83	1.18	1.31	0.14
0.2	0.75	0.59	0.83	0.97	1.14	0.16
0.2	0.5	0.59	0.83	0.8	0.99	0.19

5. CONCLUSIONS

In this paper, we have studied EUV ML blank surface roughness effect to wafer level LWR via programmed surface roughness mask. The actinic imaging results clearly showed that the surface roughness impact to LWR at large surface roughness values (Figs 7, 9, and 12). However, at the non-programmed surface roughness region, the impact of the ML RSR surface roughness to LWR is small. The current ML blank AFM surface roughness varies from 0.10-0.12nm rms. According to the correlation graph in Fig. 4, these AFM roughness value translate to ML RSR value of ~0.05-0.07nm rms. The ML surface roughness induced LWR difference for 0.05nm and 0.07nm RSR, according to Table 2, is only about 0.24nm and 0.29nm at zero focus and at 40nm defocus, respectively. When we further considering intrinsic resist LWR contribution, the total LWR improvement for resist LWR of 1.5nm and 1.0nm is only 0.1nm and 0.14nm by improving ML RSR from 0.07nm to 0.05nm, respectively. Due to the challenges of reducing resist LWR down to 1nm or below, the amount of LWR improvement by continue improving ML surface roughness from that of current POR ML blank quality will be very limited. As a result, the tradeoffs between high blank cost-of-ownership by further tightening the surface roughness specifications and limited LWR improvement need to be considered.

ACKNOWLEDGMENTS

The authors would like to thank SEMATECH for helping with ML deposition, Patrick Naulleau from LBNL for many useful discussions through out of this work, Farhad Salmassi from LBNL for Cr deposition, Robert Chen, Andy Ma, and Brittany McClinton from Intel Corporation for blank surface roughness data collection and analysis.

Measurements performed on the SHARP EUV microscope were funded by SEMATECH and conducted by the Center for X-Ray Optics at the Lawrence Berkeley National Laboratory Advanced Light Source synchrotron radiation facility. The Advanced Light Source is supported by the Director, Office of Science, Office of Basic Energy Sciences, of the U.S. Department of Energy under Contract No. DE-AC02-05CH11231.

Downloaded From: http://proceedings.spiedigitallibrary.org/ on 03/23/2015 Terms of Use: http://spiedl.org/terms

REFERENCES

1. P. Naulleau, “The relevance of mask-roughness-induced printed line-edge roughness in recent and future EUV lithography tests," Appl. Opt. 43, 4025-4032 (2004).
2. P. Naulleau and G. Gallatin, “Line-edge roughness transfer function and its application to determine mask effects in EUV resist characterization,” Appl. Opt. 42, 3390-3397 (2003).
3. B. McClinton, P. Naulleau, “Mask roughness induced LER: a rule of thumb”, Proc. of SPIE 7636 76362G (2010).
4. P. Naulleau, B. McClinton, K. Goldberg, I. Mochi, A. Rastegar, “Mask roughness challenges in extreme ultraviolet mask development,” J. Vac. Sci. & Technol. B 29, 06F501 (2011).
5. S. George,P. Naulleau, I. Mochi, F. Salmassi, E. Gullikson, K. Goldberg, and E. Anderson, “Extreme ultraviolet mask substrate surface roughness effects on lithographic patterning,” J. Vac. Sci. Technol. B 28(6), C6E23 Nov/Dec (2010).
6. S. George, P. Naulleau, I. Mochi, F. Salmassi, E. Gullikson, K. Goldberg, E. Anderson, “Replicated mask surface roughness effects on EUV lithographic patterning and line-edge roughness,” Proc. SPIE 7969, 79690E (2011).
7. K. Goldberg, I. Mochi, M. Benk, A. P. Allezy, M. R. Dickinson, C. W. Cork, D. Zehm, J. B. Macdougall, E. Anderson, F. Salmassi, W. L. Chao, V. K. Vytla, E. M. Gullikson, J. C. DePonte, M. S. Jones, D. Van Camp, J. F. Gamsby, W. B. Ghiorso, H. Huang, W. Cork, E. Martin, E. Van Every, E. Acome, V. Milanovic, R. Delano, P. P. Naulleau, and S. B. Rekawa, "Commissioning an EUV mask microscope for lithography generations reaching 8 nm," Proc. of SPIE 8679, 867919 (2013).
8. A. Vaglio Pret, R. Gronheida , T. Younkin, M. Leeson , P. Y. Yan, “Impact of EUV Mask Surface Roughness on LER,” Proc. of SPIE Vol. 8322 83220N-1, (2012).
9. S. Bhattarai, A. Neureuther; P. Naulleau “Limitations of resist-based characterization of EUV mask surface roughness,” Proc. SPIE. Vol 9048, 904837 (2014).
10. International Technology Roadmap for Semiconductors, 2013ed, http://public.itrs.net/.
11. D. Wintz, K. Goldberg, I. Mochi, S. Huh, "Photon flux requirements for EUV-reticle imaging microscopy in the 22- and 16-nm nodes," Proc. of SPIE 7636, 76362L (2010).

Downloaded From: http://proceedings.spiedigitallibrary.org/ on 03/23/2015 Terms of Use: http://spiedl.org/terms